A Novel Deadbeat Predictive Current Control Scheme for OEW-PMSM Drives

Xin Yuan, Chengning Zhang, and Shuo Zhang, *Member, IEEE*

***Abstract*—In an open-end winding permanent magnet synchronous machines drive with single dc voltage source, zero-sequence current (ZSC) can lead to a high current stress of power modules and loss of motor. Therefore, some modulation strategies have been employed to alleviate ZSC by suppressing zero-sequence voltage (ZSV). However, ZSC still exists in the system because ZSV can also be generated by other nonlinear factors of inverter such as the dead time of system. In addition, zero-sequence back electromotive force in the zero-sequence path can also enlarge torque ripple and ZSC. In order to deal with above problems, first, this paper proposes a full-order adaptive zero-sequence observer to estimate future ZSC and ZSV, which are able to compensate one-step control delay. Second, to achieve the maximum voltage dc bus utilization, this paper proposes a novel deadbeat predictive current control (DPCC) scheme with alternate sub-hexagonal center pulsewidth modulation strategy to suppress ZSC and torque ripple simultaneously. Finally, this paper presents a comparative study of two types of methods, namely traditional DPCC scheme and the proposed DPCC scheme. Simulation and experimental results are demonstrated to verify the effectiveness of the proposed DPCC scheme.**

***Index Terms*—Deadbeat predictive current control (DPCC), open-end winding permanent magnet synchronous machines (OEW-PMSMs), zero-sequence current suppression.**

I. Introduction

RECENTLY, permanent magnet synchronous machines (PMSMs) get extensive attention in the modern applications because PMSMs have many advantages such as high efficiency and high torque density. To obtain a higher speed, flux-weakening control method needs to be carried out but it may lead to a poor efficiency in flux-weakening field and degauss permanent magnets when the system is out of control. The work in [1] shows that open-end winding PMSMs (OEW-PMSMs) with dual voltage source inverter (VSI) can overcome the aforementioned problems. OEW-PMSMs have six terminals of stator windings available and they are able to expand the motor speed range and enhance the system reliability.

Manuscript received October 7, 2018; revised November 23, 2018 and January 8, 2019; accepted March 7, 2019. Date of publication March 10, 2019; date of current version September 6, 2019. This work was supported by the National Natural Science Foundation of China under Grant 51677005. Recommended for publication by Associate Editor A. M. Trzynadlowski. *(Corresponding author: Chengning Zhang.)*

The authors are with the School of Mechanical Engineering and the Collaborative Innovation Center of Electric Vehicles in Beijing, Beijing Institute of Technology, Beijing 100081, China (e-mail:

PI current control has lower torque ripples. However, the tuning of the proportion and integral parameter is time-consuming. Recently, predictive current control is widely used in PMSMs drives due to the excellent response performance [15]. There are two sorts of predictive current control, namely finite control set-model predictive current control (FCS-MPCC) [16] and deadbeat predictive current control (DPCC). In terms of the steady performance, DPCC is better than FCS-MPCC due to much more voltage vectors available. Since the mathematical model of OWE-PMSMs is similar to that of PMSMs, many researchers have applied predictive current control in the field of OEW-PMSMs. The work in [17] establishes a current-error-based cost function to suppress ZSC, which includes a *dq*-axis current error and ZSC error. However, it is applied in a semi controlled OEW-generation system. The work in [18] proposes a predictive torque control scheme to control OEW-induction motor, and the tuning weighting factor assignment is avoided. To reduce the calculation burden in FCS-MPCC, the work in [19] proposes a fast voltage selection FCS-MPCC scheme for OEW-PMSMs control. To reduce torque ripples and ZSC, the work in [20] proposes a modified predictive current control based on an A-B-C frame, without using cost function in OEW-induction motor.

Besides the effect of ZSV on ZSC, zero-sequence back electromotive force (EMF) can also be regarded as the major disturbance source of OEW-PMSMs [21]. Considering the influence of zero-sequence EMF on torque ripples, the work in [22] injects an extra fluctuating component in the *q*-axis current and an additional torque can be generated to counteract the torque ripples caused by zero-sequence EMF. However, this reference does not suppress the ZSC caused by the dead time of system. The work in [23] proposes a phase-locked loop-based position observer to evaluate zero-sequence EMF, but it is time-consuming. Considering the influence of the dead time of inverter on ZSC, the work in [24] proposes a dual-space vector control scheme with SHCPWM, which utilizes a PI regulator to suppress ZSC, but this reference does not consider the suppression of torque ripples caused by zero-sequence EMF and is only applied in the PI current control scheme.

B. Motivation and Innovation

Generally, central hexagon PWM modulation and SHCPWM are popular in OEW-PMSMs drive with single dc voltage inverter. From the view of switching loss reduction, SHCPWM is better because the two inverters' switching times change from 12 times to 6 times within each control period. In addition, although central hexagon PWM modulation can eliminate ZSV, some nonlinear factors of inverter such as the dead time of system can also generate ZSV, which can augment ZSC. Furthermore, the maximum voltage dc bus utilization cannot be achieved. Therefore, this paper adopts SHCPWM in OEW-PMSMs.

However, SHCPWM will generate ZSV within each control period and zero-sequence EMF exist in the zero-sequence path of system, which can enlarge torque ripple. In order to overcome the aforementioned drawbacks, three contributions would be presented in this paper.

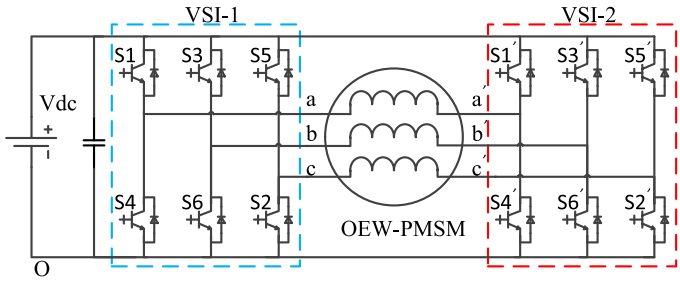

Fig. 1. Single dc voltage source dual-VSI fed OEW-PMSM.

1) Since a practical system has one-step delay, ZSC and ZSV at the $(k+1)$th instant need to be obtained to pursuit a better performance for suppressing ZSC and torque ripple. Thus, this paper proposes a full-order adaptive zero-sequence observer (ZSO) to predict ZSV and ZSC at the $(k+1)$th instant simultaneously.
2) Different from the previous methods for ZSC and torque ripple suppression, this paper proposes a novel DPCC scheme with ZSO.
3) Simulation and experiment results can be demonstrated to verify the correctness of the proposed DPCC scheme under different conditions.

C. Paper Organization

This paper is organized as follows. Section II illustrates the basic structure of OEW-PMSM drive with single dc voltage source. Then, the proposed DPCC scheme with SHCPWM is shown in Section III. To testify the correctness of the proposed method, Sections IV and V present simulation and experimental results for the two methods, namely the traditional DPCC scheme with SHCPWM and proposed DPCC scheme with SHCPWM. Finally, the conclusions are presented in Section VI.

II. OEW-PMSM Drive With Single DC Voltage

A. Dual-VSI Fed OEW-PMSM

Aiming to study OEW-PMSMs drive with single dc voltage source, the topology is illustrated in Fig. 1. From this figure, the two-level inverter is adopted as a VSI. In this circuit, each of VSI independently obtains eight switching combinations and the voltage vector of VSI-1 U_{s1} and VSI-2 U_{s2} can be presented in the following equation:

$$\begin{cases} U_{s1} = \dfrac{2}{3}\left(u_{ao} + e^{j\frac{2\pi}{3}}u_{bo} + e^{j\frac{4\pi}{3}}u_{co}\right) \\ U_{s2} = \dfrac{2}{3}\left(u_{a'o} + e^{j\frac{2\pi}{3}}u_{b'o} + e^{j\frac{4\pi}{3}}u_{c'o}\right) \end{cases} \tag{1}$$

where subscript $a^{'}$, $b^{'}$, $c^{'}$, *a, b,* and *c* denote the motor $a^{'}$, $b^{'}$, $c^{'}$, *a, b,* and *c* phase; $u_{xo}\,(x = a^{'}, b^{'}, c^{'}, a, b, c)$ denotes the voltage from *x* phase to *O* point. Three phase stator voltages for OEW-PMSM can be expressed as follows:

$$\begin{cases} u_a = u_{aa'} = u_{ao} - u_{a'o} \\ u_b = u_{bb'} = u_{bo} - u_{b'o} \\ u_c = u_{cc'} = u_{co} - u_{c'o} \end{cases} \tag{2}$$

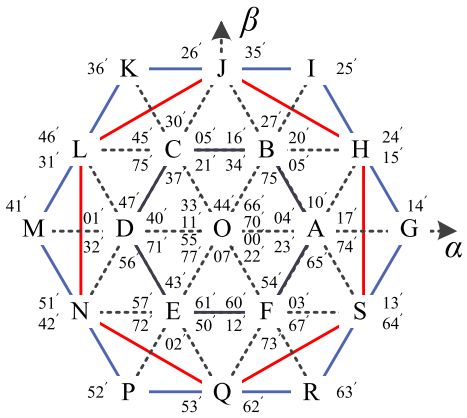

Fig. 2. Space voltage vector diagram for dual-VSI.

where u_a, u_b, and u_c denote the *a*, *b,* and *c* phase stator voltages. According to (1) and (2), the stator voltage U_s in an $\alpha\beta$ stationary frame for OEW-PMSM can be expressed as follows:

$$U_s = U_{s1} - U_{s2}. \tag{3}$$

To analyze the cause for ZSV, ZSV can be expressed as follows:

$$U_0 = \frac{u_a + u_b + u_c}{3} \tag{4}$$

where U_0 denotes ZSV of OEW-PMSM. ZSC can be expressed in the following equation:

$$i_0 = \frac{i_a + i_b + i_c}{3} \tag{5}$$

where i_a, i_b, and i_c denote the *a*, *b*, and *c* phase stator currents; i_0 denotes ZSC.

According to the aforementioned analysis, total possible switching combinations in the dual-VSI fed OEW-PMSM can reach to 64 ($2^3 \times 2^3$),which can generate 18 different non-zero voltage vectors and one zero voltage vector. This topology is similar to that of three-level inverters. Fig. 2 shows the space voltage vectors in dual-VSI in the α β stationary frame. The zero voltage vector locates at the origin O, and 18 non-zero voltage vectors are distributed on the vertexes of three hexagons, namely ABCDEF, HJLNQS, and GIKMPR. The reference voltage vector can be synthesized by these voltage vectors and the maximum modulation indexes of the three hexagons are approximate to 0.57735, 1, and 1.15470, respectively. An *et al*. in [24] have noted that the seven switching combinations on the vertexes of the hexagons HJLNQS can avoid ZSV and utilize two adjacent voltage vectors on HJLNQS to synthetize the reference voltage vector. Both adjacent voltage vectors would be obtained through space vector PWM (SVPWM) in each VSI. However, the maximum modulation index is 1 and the maximum voltage dc bus utilization cannot be achieved in dual-VSI.

B. Mathematical Model of OEW-PMSM

The surface mounted type OEW-PMSM is studied in this paper, which means that the inductance L_d in the *d*-axis is equal to the inductance L_q in the *q*-axis. In addition, because the third harmonic back EMF is larger than the higher order harmonic

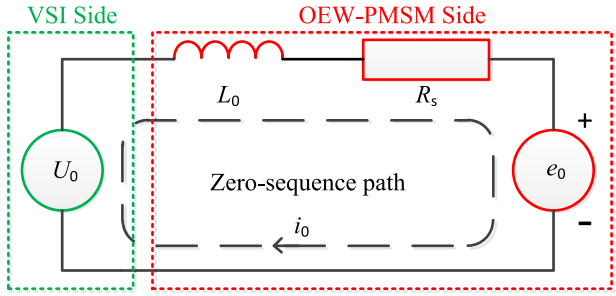

Fig. 3. Zero-sequence path of OEW-PMSM.

back EMF, this paper assumes that the zero-sequence back EMF is all caused by the third harmonic flux linkage. In this case, the equivalent circuit of zero-sequence path is shown in Fig. 3. To simplify the OEW-PMSM model, some trivial OEW-PMSM parameters are ignored such as copper loss, iron loss, and so forth. The mathematical model of OEW-PMSM equations in the $\alpha\beta 0$ stationary frame can be presented as follows:

$$U_s = R_s i_s + \frac{d\psi_s}{dt} \tag{6}$$

$$e_0 = 3\omega_e \psi_{3f} \sin(3\theta_r) \tag{7}$$

$$U_0 = R_s i_0 + L_0 \frac{di_0}{dt} + e_0 \tag{8}$$

$$\psi_s = L_s i_s + \psi_f e^{j\theta_r} \tag{9}$$

$$T_e = 1.5p\left(\psi_f i_q - 6\psi_{3f} \sin(3\theta_r) i_0\right) \tag{10}$$

where R_s, L_s, and Ψ_f denote the stator resistance, stator inductance, and rotor fundamental flux linkage, respectively; ω_e denotes the electrical angular frequency; i_s and U_s stand for the stator current vector and stator voltage vector, respectively; U_0 and i_0 denote ZSV and ZSC, respectively; L_0 and Ψ_{3f} denote the zero-sequence inductances and rotor flux linkage (the third harmonic flux linkage); p and θ_r are the number of pole pairs and electrical rotor angle, respectively; Ψ_s denotes the stator flux linkage vector; e_0 denotes the zero-sequence EMF; T_e denotes the electromagnetic torque. Zhan *et al*. in [23] have noted that L_0 can be obtained as follows:

$$L_0 = L_s - 2M_s \tag{11}$$

where M_s represents the mutual inductance between any two motor phases. The mechanical equation of OEW-PMSM can be expressed as follows:

$$T_e - T_l = \eta \frac{d\omega_m}{dt} \tag{12}$$

where η stands for the motor inertia; ω_m and T_l stand for the mechanical rotor angular frequency and load torque.

III. Proposed DPCC Scheme for OEW-PMSM Drive

First, the traditional DPCC scheme with SHCPWM will be presented in Section III-A. Second, Section III-B will introduce the proposed DPCC scheme with ZSC and torque ripple suppression.

A. Traditional DPCC Scheme With SCHPWM for OEW-PMSM Drive

According to (6) and (9), the OEW-PMSM voltage equation in the $\alpha\beta 0$ stationary frame is presented as follows:

$$U_s = R_s i_s + L_s \frac{di_s}{dt} + j\psi_f \omega_m p e^{j\theta_r}. \tag{13}$$

In the practical system, the system sampling time is discrete, thus this paper adopts the first-order Euler discretization to obtain the reference voltage vector, which can be expressed as follows:

$$U_s(k) = R_s i_s(k) + L_s \frac{i_s{}^{\text{ref}}(k+1) - i_s(k)}{T_s} + j\psi_f \omega_m(k) p e^{j\theta_r(k)} \tag{14}$$

where T_s denotes the sampling period; $i_s{}^{\text{ref}}(k+1)$ denotes the reference current at the $(k+1)$th instant. The principle of DPCC is to obtain the reference voltage vector that forces the actual current vector to track the reference current according to (14). Since the sampling period is quite short, the variation of θ_r between at the $(k+1)$th instant and at the kth instant is neglected. In addition, the reference current at the $(k+1)$th instant can be approximately presented as follows:

$$i_s{}^{\text{ref}}(k+1) = i_s{}^{\text{ref}}(k). \tag{15}$$

Since the system has one-step delay, the delay compensation should be adopted [26]. The stator current $i_s(k+1)$ at the $(k+1)$th instant can be expressed as follows:

$$i_s(k+1) = i_s(k) + \frac{T_s}{L_s} \left(U_s(k)^* - R_s i_s(k) - j\psi_f \omega_m(k) p e^{j\theta_r(k)} \right) \tag{16}$$

where $U_s(\mathrm{k})^*$ denotes the obtained voltage vectors at the kth instant. After obtaining the stator currents $i_s(k+1)$, the voltage equation at the $k+1$th instant can be expressed as follows:

$$U_s(k+1) = \frac{L_s}{T_s} i_s{}^{\text{ref}}(k) - \frac{L_s}{T_s} i_s(k+1) + R_s i_s(k+1) + j\psi_f \omega_m(k) p e^{j\theta_r(k)}. \tag{17}$$

Substituting (16) in (7), the reference voltage vectors at the $(k+1)$th instant can be obtained.

Different from [8], to achieve the maximum voltage utilization and reduce system switching frequency, SHCPWM strategy has been employed in [10] and [25]. The alternate sub-hexagonal center PWM modulation diagram is shown in Fig. 4. In Fig. 4, we can find that there are six sectors in SHCPWM, namely sectors I, II, III, IV, V, and VI. When the reference voltage is located in sectors I, III, and IV, the voltage vector in VSI-1 is generated by a fixed switching state and the voltage vector in VSI-2 is synthesized by space vector PWM. Whereas, when the reference voltage is located in sectors II, IV, and VI, the voltage vector in VSI-1 is synthesized by space vector PWM and voltage vector in VSI-2 is generated by a fixed switching state.

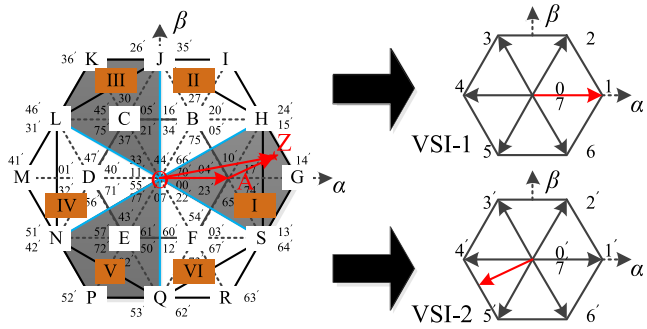

Fig. 4. Alternate sub-hexagonal center PWM diagram for dual-VSI.

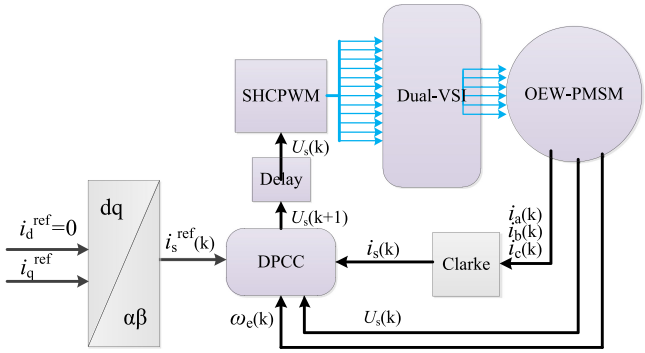

Fig. 5. Traditional DPCC scheme with SHCPWM for OEW-PMSM drive.

For example, in Fig. 4, when the reference voltage vector **OZ** is located in sector I, the vector **OA** in VSI-1 would be clamped for one control period. Due to **OZ** = **OA** + **AZ**, the vector **AZ** can be synthesized through space vector PWM in VSI-2. In this case, the two inverters' switching times change from 12 times to 6 times and the maximum voltage dc bus utilization can be achieved. The DPCC scheme with SHCPWM for the OEW-PMSM drive can be presented in Fig. 5.

B. Proposed DPCC Scheme With ZSC and Torque Ripple Suppression

However, the traditional DPCC method with SHCPWM will generate ZSC and the motor torque ripple will be augmented. To deal with the aforementioned problems, some scholars present many methods but few methods are proposed in the field of DPCC. The work in [11] analyzes the effect of zero-vector placement for SHCPWM on ZSV. Except for the effect of ZSV on the ZSC and torque ripples, the third harmonic back EMF is a major factor to deteriorate the ZSC and torque ripple. Therefore, first, this paper proposes a ZSO based on adaptive sliding mode control (SMC) to predict ZSV and ZSC simultaneously at the $k+1$th instant. After obtaining ZSV and ZSC at the $k+1$th instant, this paper proposes a novel DPCC scheme with SHCPWM. In the proposed DPCC scheme, ZSC can be suppressed and the compensatory current i_{q0} will be obtained and applied to reduce the torque ripples caused by the third harmonic back EMF.

Based on the sliding mode theory, the specific procedures of ZSO are presented as follows.

1) ZSC i_0 is used as controlled variables. To avoid the switching chatting and make the i_0 error approach to zero

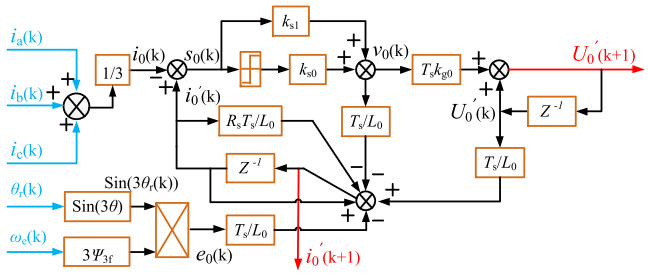

Fig. 6. Discrete block diagram of ZSO.

quickly, the sliding mode surface s_0 can be designed as follows:

$$s_0 = i_0' - i_0 \tag{18}$$

where i_0', i_0, and s_0 denote the estimates of ZSC, measured ZSC, and sliding mode surface, respectively.

2) Different from the traditional sliding mode function, the sliding mode function v_0 is designed as follows:

$$v_0 = k_{s0}\text{sign}(s_0) + k_{s1}s_0 \tag{19}$$

$$\text{sign}(s) = \begin{cases} 1 & \text{if } (s > 0) \\ 0 & \text{if} (s = 0) \\ -1 & \text{if} (s < 0) \end{cases} \tag{20}$$

where k_{s0} and k_{s1} denote the adaptive SMC parameters.

3) After obtaining the sliding mode function, the ZSO equation can be expressed as follows:

$$\begin{cases} U_0' = R_s i_0' + L_0 \dfrac{di_0'}{dt} + e_0 + v_0 \\ \dfrac{dU_0'}{dt} = k_{g0} v_0 \end{cases} \tag{21}$$

where U_0' and k_{g0} denote the estimates of ZSV and adaptive SMC parameter. Because the proposed ZSO will be performed at discrete instant, the discrete expression of ZSO can be expressed in (22) and the discrete block diagram of ZSO is illustrated in Fig. 6

$$\begin{cases} i_0'(k+1) = \dfrac{T_s}{L_0}(U_0'(k) - R_s i_0'(k) - e_0(k) \\ \qquad\qquad -v_0(k)) + i_0'(k) \\ U_0'(k+1) = U_0'(k) + T_s k_{g0} v_0(k). \end{cases} \tag{22}$$

Because the adaptive SMC system is a type of nonlinear control, sometimes the system may be unstable. To testify the stability of ZSO, this paper utilizes the Lyapunov theorem to ensure the convergence property of the adaptive SMC. The Lyapunov function V is expressed as follows:

$$V = \frac{1}{2}{s_0}^2. \tag{23}$$

Based on the Lyapunov stability principle, the following equation can be expressed:

$$\frac{dV}{dt} = s_0 \frac{ds_0}{dt} \le 0. \tag{24}$$

Subtracting (8) from (21), the equation can be illustrated as follows:

$$U_0' - U_0 = R_s s_0 + L_0 \frac{ds_0}{dt} + v_0. \tag{25}$$

According to (19), the sliding mode surface s_0 equation is obtained as follows:

$$\begin{aligned} s_0 \frac{ds_0}{dt} &= \frac{1}{L_0}\left(s_0(U_0' - U_0 - k_{s0}\text{sign}(s_0)) - k_{s1}{s_0}^2 - R_s{s_0}^2\right) \\ &= \begin{cases} \dfrac{1}{L_0}(s_0(U_0' - U_0 - k_{s0}) \\ \quad -k_{s1}{s_0}^2 - R_s{s_0}^2), & s_0 > 0 \\ \dfrac{1}{L_0}(s_0(U_0' - U_0 + k_{s0}) \\ \quad -k_{s1}{s_0}^2 - R_s{s_0}^2), & s_0 < 0 \\ 0, & s_0 = 0. \end{cases} \end{aligned} \tag{26}$$

To ensure the convergence property of the adaptive SMC, the k_{s0} and k_{s1} need to be satisfied as follows:

$$\begin{cases} k_{s0} > \|U_0' - U_0\| \\ k_{s1} > -R_s \ . \end{cases} \tag{27}$$

After establishing ZSO, it can be found that the electromagnetic torque may be fluctuant due to the third harmonic back EMF in the following equation:

$$T_e = 1.5p\left(\psi_f i_q - 6\psi_{3f}\sin(3\theta_r) i_0\right). \tag{28}$$

To suppress the torque ripple caused by the third harmonic back EMF, (28) can be turned into (29), which can be expressed as follows:

$$\begin{aligned} T_e &= 1.5p\left(\psi_f(i_{q1} + i_{q0}) - 6\psi_{3f}\sin(3\theta_r) i_0\right) \\ &= 1.5p\left(\psi_f i_{q1}\right) + 1.5p\left(\psi_f i_{q0} - 6\psi_{3f}\sin(3\theta_r) i_0\right) \end{aligned} \tag{29}$$

where i_{q0} denotes the compensatory current. Assuming that the torque produced by i_{q0} can counteract the fluctuant torque ripple produced by the zero-sequence EMF, which can be expressed as follows:

$$\psi_f i_{q0} = 6\psi_{3f}\sin(3\theta_r) i_0. \tag{30}$$

The compensatory current i_{q0} is obtained as follows:

$$i_{q0} = i_0 \frac{6\psi_{3f}\sin(3\theta_r)}{\psi_f}. \tag{31}$$

Thus, the reference current ${i_q}^{\text{Modref}}(k+1)$ can be modified as follows:

$${i_q}^{\text{Modref}}(k+1) = {i_q}^{\text{ref}}(k+1) + i_{q0}(k+1). \tag{32}$$

Since ZSC i_0 at the $(k+1)$th instant has been obtained through the output of ZSO, the compensatory current $i_{q0}(k+1)$ can be obtained. According to (31), the reference current

$i_q^{\text{Modref}}(k+1)$ can be expressed as follows:

$$i_q^{\text{Modref}}(k+1) = i_q^{\text{ref}}(k+1) + i_0'(k+1)\frac{6\psi_{3f}\sin(3\theta_r(k+1))}{\psi_f}$$
$$\approx i_q^{\text{ref}}(k) + i_0'(k+1)\frac{6\psi_{3f}\sin(3\theta_r(k))}{\psi_f}. \tag{33}$$

In terms of the traditional SHCPWM, U_s voltage vector may generate ZSV and ZSV will augment ZSC. Therefore, SHCPWM with zero-vector placement is employed to suppress the ZSC. The specific procedure is presented as follows.

1) Judgment of the sector needs to be performed. The reference voltage vector in $\alpha\ \beta$ stationary frame is transformed to abc frame, which is presented as follows:

$$\begin{cases} u_{\text{ref}a} = u_{\text{ref}\alpha} \\ u_{\text{ref}b} = -\dfrac{\left(u_{\text{ref}\alpha} - \sqrt{3}u_{\text{ref}\beta}\right)}{2} \\ u_{\text{ref}c} = -\dfrac{\left(u_{\text{ref}\alpha} + \sqrt{3}u_{\text{ref}\beta}\right)}{2} \end{cases} \tag{34}$$

where $u_{\text{ref}a}$, $u_{\text{ref}b}$, and $u_{\text{ref}c}$ denote the reference voltage in the *abc* frame; $u_{\text{ref}\alpha}$ and $u_{\text{ref}\beta}$ denote the reference voltage in the $\alpha\ \beta$ frame.

2) The reference voltage vector **OZ** needs to be synthesized by **OZ** = **OX** + **XZ**, X ∈ (A, B, C, D, E, F). Like the aforementioned analysis in Fig. 4, the voltage vectors **OX** and **XZ** are obtained as follows:

$$\begin{cases} \text{I}: \begin{cases} u_{\text{ref}\alpha 1} = 2V_{\text{dc}}/3, u_{\text{ref}\beta 1} = 0; \\ u_{\text{ref}\alpha 2} = -\left(u_{\text{ref}\alpha} - 2V_{\text{dc}}/3\right), \\ u_{\text{ref}\beta 2} = -u_{\text{ref}\beta}; \end{cases} \\ \text{II}: \begin{cases} u_{\text{ref}\alpha 1} = u_{\text{ref}\alpha} - V_{dc}/3, \\ u_{\text{ref}\beta 1} = u_{\text{ref}\beta} - \sqrt{3}V_{\text{dc}}/3; \\ u_{\text{ref}\alpha 2} = -V_{\text{dc}}/3, \\ u_{\text{ref}\beta 2} = -\sqrt{3}V_{\text{dc}}/3; \end{cases} \\ \text{III}: \begin{cases} u_{\text{ref}\alpha 1} = -V_{\text{dc}}/3, \\ u_{\text{ref}\beta 1} = \sqrt{3}V_{\text{dc}}/3; \\ u_{\text{ref}\alpha 2} = -\left(u_{\text{ref}\alpha} + V_{\text{dc}}/3\right), \\ u_{\text{ref}\beta 2} = -\left(u_{\text{ref}\beta} - \sqrt{3}V_{\text{dc}}/3\right); \end{cases} \\ \text{IV}: \begin{cases} u_{\text{ref}\alpha 1} = u_{\text{ref}\alpha} + 2V_{\text{dc}}/3, \\ u_{\text{ref}\beta 1} = u_{\text{ref}\beta}; \\ u_{\text{ref}\alpha 2} = 2V_{\text{dc}}/3, \\ u_{\text{ref}\beta 2} = 0; \end{cases} \\ \text{V}: \begin{cases} u_{\text{ref}\alpha 1} = -V_{\text{dc}}/3, \\ u_{\text{ref}\beta 1} = -\sqrt{3}V_{\text{dc}}/3; \\ u_{\text{ref}\alpha 2} = -\left(u_{\text{ref}\alpha} + V_{\text{dc}}/3\right), \\ u_{\text{ref}\beta 2} = -\left(u_{\text{ref}\beta} + \sqrt{3}V_{\text{dc}}/3\right); \end{cases} \\ \text{VI}: \begin{cases} u_{\text{ref}\alpha 1} = u_{\text{ref}\alpha} - V_{\text{dc}}/3, \\ u_{\text{ref}\beta 1} = u_{\text{ref}\beta} + \sqrt{3}V_{\text{dc}}/3; \\ u_{\text{ref}\alpha 2} = -V_{\text{dc}}/3, \\ u_{\text{ref}\beta 2} = \sqrt{3}V_{\text{dc}}/3. \end{cases} \end{cases} \tag{35}$$

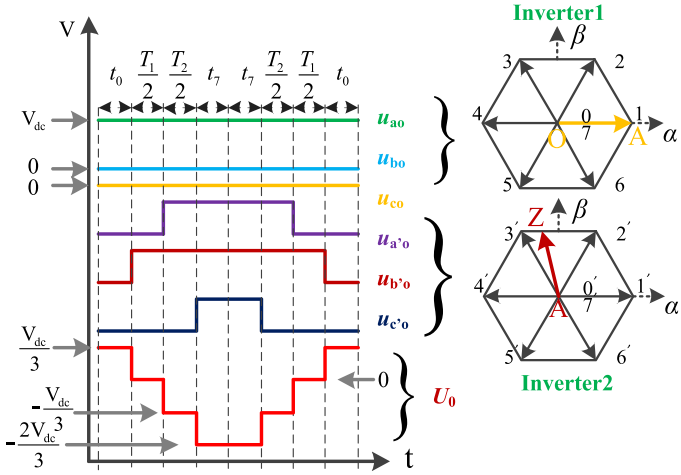

Fig. 7. Zero-sequence voltage waveform within one control period.

TABLE I
T_1 AND T_2 COMPUTATIONS FOR DIFFERENT SECTORS

Sector	U_1, U_2	U_2, U_3	U_3, U_4	U_4, U_5	U_5, U_6	U_6, U_1
T_1	-Z	Z	X	-X	-Y	Y
T_2	X	Y	-Y	Z	-Z	-X

3) To suppress ZSC, the appropriate distribution factor x_{zero} of zero vectors needs to be designed according to the value of U_0'. For example, when the applied voltage U_s is in sector I according to (35), **OA** and **AZ** can be regarded as the applied voltage in inverter 1 and inverter 2 respectively. If **AZ** is in the second sector, the zero-sequence voltage waveform within one control period can be presented in Fig. 7. The duration time T_0 for which the zero vectors is applied can be obtained as follows:

$$T_0 = T_s - T_1 - T_2 \tag{36}$$

where T_s is the system control period; T_1 and T_2 are the respective duration time for which two adjacent voltage vectors are applied within each control period. To calculate T_1 and T_2, three variables *X*, *Y*, and *Z* are defined as follows:

$$X = \frac{T_s U\text{ref}\beta}{V\text{dc}/\sqrt{3}}$$
$$Y = \frac{\sqrt{3}T_s U\text{ref}\beta}{2V\text{dc}} + \frac{3T_s U\text{ref}\alpha}{2V\text{dc}}$$
$$Z = \frac{\sqrt{3}T_s U\text{ref}\beta}{2V\text{dc}} - \frac{3T_s U\text{ref}\alpha}{2V\text{dc}} \tag{37}$$

where $U_{\text{ref}\alpha}$ and $U_{\text{ref}\beta}$ denote the synthetic reference voltage vector **XZ** in the $\alpha\ \beta$ frame. For different sectors, the expressions for T_1 and T_2 are presented in Table I. The duration time T_0 is evenly divided into four parts, namely two duration time t_0 and two duration time t_7. t_0 and t_7

TABLE II
RIGHT DUTY CYCLE FOR INVERTER IN DIFFERENT SECTORS

Sector	U_1, U_2	U_2, U_3	U_3, U_4	U_4, U_5	U_5, U_6	U_6, U_1
T_a	T_{aon}	T_{bon}	T_{bon}	T_{con}	T_{con}	T_{aon}
T_b	T_{bon}	T_{aon}	T_{con}	T_{bon}	T_{aon}	T_{con}
T_c	T_{con}	T_{con}	T_{aon}	T_{aon}	T_{bon}	T_{bon}

can be obtained in the following equation:

$$\begin{cases} t_0 = \dfrac{T_0 x_{\text{zero}}}{4} \\ t_7 = \dfrac{2T_0 - T_0 x_{\text{zero}}}{4}. \end{cases} \tag{38}$$

In Fig. 7, it can be found that the value of ZSV is $V_{\text{dc}}/3$ during time t_0 and the value of ZSV is $-2V_{\text{dc}}/3$ during time t_7. Therefore, the average values of ZSV within one control period can be generated according to different x_{zero} and U_s. Because the predicted ZSV U_0' at the $(k+1)$th instant can be obtained through the proposed ZSO, to suppress ZSC, the average ZSV at the kth instant needs to counteract the value of ZSV at the $(k+1)$th instant. According to the principle of volt-second balance, the equation can be expressed as follows:

$$\begin{aligned} T_s U_0' &= -\left(\frac{T_0 x_{\text{zero}}}{2}\frac{V_{\text{dc}}}{3} - \frac{2V_{\text{dc}}}{3}\left(T_0 - \frac{T_0 x_{\text{zero}}}{2}\right) - \frac{V_{\text{dc}}}{3}T_2\right) \\ &= -\frac{V_{\text{dc}}}{3}\left(\frac{3T_0 x_{\text{zero}}}{2} - 2T_0 - T_2\right). \end{aligned} \tag{39}$$

According to (39), the appropriate distribution factor x_{zero} can be obtained as follows:

$$x_{\text{zero}} = -\frac{2U_0' T_s}{V_{\text{dc}} T_0} + \frac{4}{3} + \frac{2T_2}{3T_0}. \tag{40}$$

4) Determination of the duty cycle T_{aon}, T_{bon}, and T_{con} needs to be performed, which can be presented as follows:

$$\begin{cases} T_{aon} = \dfrac{T_0}{2T_s} x_{\text{zero}} \\ T_{bon} = T_{aon} + \dfrac{T_1}{T_s} \\ T_{con} = T_{bon} + \dfrac{T_2}{T_1}. \end{cases} \tag{41}$$

5) After the right duty cycle is assigned to the inverter, according to different sectors, the right duty cycle for the inverter is presented in Table II. Therefore, the proposed DPCC scheme with ZSC and torque ripple suppression would be presented in Fig. 8.

IV. SIMULATION STUDY

The simulation model for OEW-PMSM drive system is established in MATLAB software and the OEW-PMSM parameters are listed in Table III. To approach the practical condition in simulation, the dead time model is built and the dead time is set to 2.5 μs. In addition, the third harmonic back EMF is added into the system and 50 μs is set as the system control period. Two methods will be compared in this paper, namely the traditional DPCC method (method 1) and the proposed DPCC method (method 2). The closed-loop speed control all adopts PI control in the two methods and the PI proportionality coefficient and integral coefficient are 1.56 and 0.24, respectively. In the proposed DPCC method, the adaptive SMC parameters k_{s0}, k_{s1}, and k_{g0} are 80, 80, and –7000, respectively.

First, the ZSC suppression performance will be observed. Fig. 9 shows that ZSC i_0 and ZSV U_0 with 5 kHz cutoff

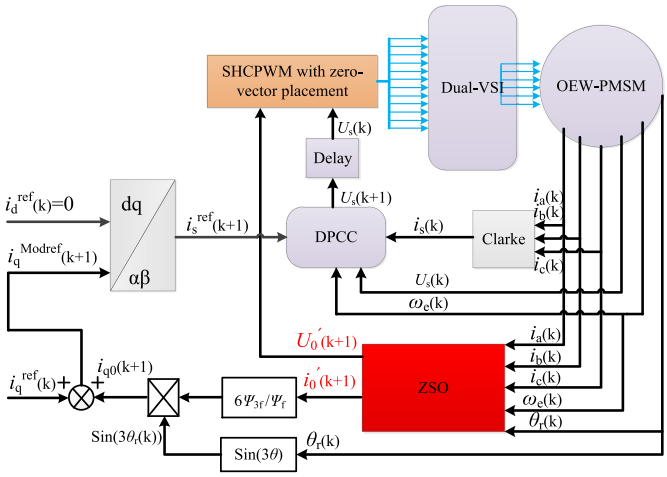

Fig. 8. Proposed DPCC scheme with ZSC and torque ripple suppression for OEW-PMSM drive.

TABLE III
OEW-PMSM PARAMETERS

Parameter	Description	Value
P_N	Rated power (kW)	1
p	Number of pole pairs	4
R_S	Stator resistance (Ω)	1.38
L_S	Stator inductance (mH)	3.21
L_0	Zero-sequence inductance (mH)	3.1
I_N	Rated current (A)	4
T_N	Rated torque (Nm)	4
Ψ_{3f}	The third rotor flux linkage (Wb)	0.0074
Ψ_f	Rotor flux linkage (Wb)	0.1667

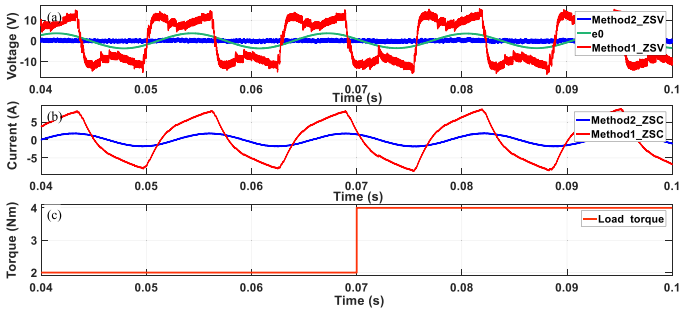

Fig. 9. Simulation results of ZSC i_0 and ZSV U_0 with 5 kHz cutoff frequency performance at 400 r/min. (a) ZSV U_0 and zero-sequence back EMF e_0. (b) ZSC i_0. (c) Load torque T_l.

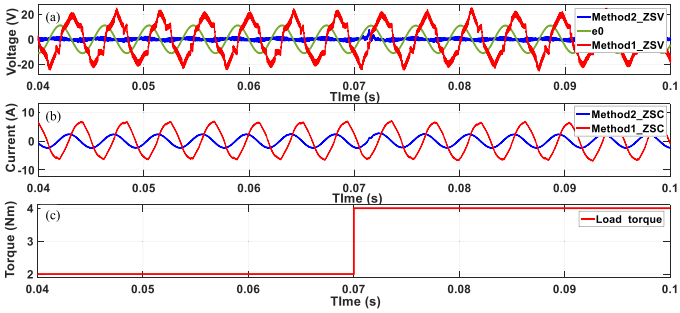

Fig. 10. Simulation results of ZSC i_0 and ZSV U_0 with 5 kHz cutoff frequency performance at 1200 r/min. (a) ZSV U_0 and zero-sequence back EMF e_0. (b) ZSC i_0. (c) Load torque T_l.

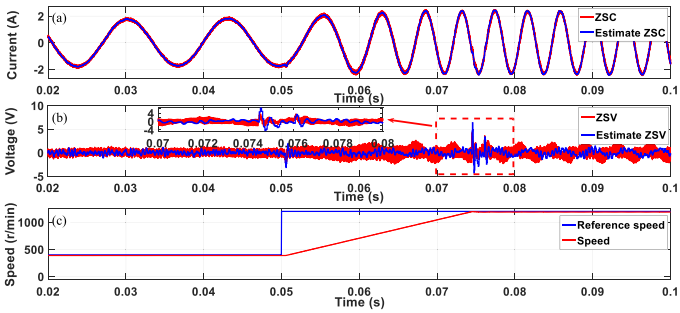

Fig. 11. Simulation results of the estimates of ZSC i_0 and ZSV U_0 with 5 kHz cutoff frequency comparison from 400 to 1200 r/min in method 2. (a) ZSC and estimate of ZSC. (b) ZSV and estimate of ZSV. (c) Motor speed and reference motor speed.

frequency and zero-sequence back EMF e_0 performance of the two methods at 400 r/min and the load torque change from 2 to 4 N·m. From this figure, it can be found that the proposed DPCC method can suppress ZSC effectively. In addition, ZSC i_0 and ZSV U_0 with 5 kHz cutoff frequency and zero-sequence back EMF e_0 performance of the two methods at 1200 r/min is presented in Fig. 10. It can be found that the amplitude of the ZSC and ZSV in the proposed DPCC method is lower than that of the traditional DPCC method, which means that the proposed DPCC method have the ability of ZSC suppression in the low speed and high speed region, respectively. It should be noted that the zero-sequence EMF effect on ZSC at 1200 r/min is obvious because the value of the zero-sequence back EMF is higher with the speed rising. In Fig. 11, we can find that the estimates of ZSC and ZSV are able to track the actual ZSC and ZSV with 5 kHz cutoff frequency performance in different speed conditions, which testifies the correctness of the proposed ZSO.

Second, to testify the correctness of torque ripple suppression in the proposed method, the load torque is set to 2 N·m at 0 s and up to 4 N·m at 0.04 s and then down to 1 N·m at 0.07 s. It can be seen that the fluctuation of the d-axis and q-axis currents has been decreased compared with the traditional DPCC method in Fig. 12. In addition, because the system contains the speed closed-loop control, the speed fluctuation of method 2 is reduced. Fig. 13 shows the electromagnetic torque T_e and fluctuant torque ripple T_0 produced by the zero-sequence EMF performance of the two methods. It can be seen that these torque ripples are reduced because the compensatory current

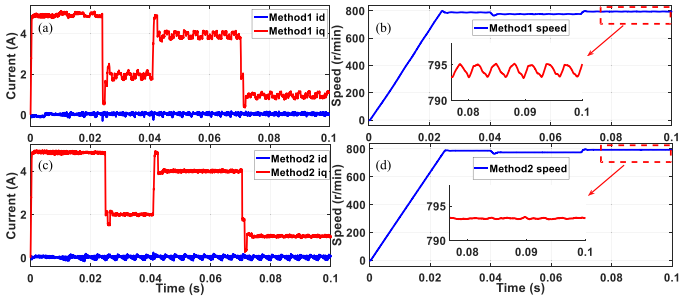

Fig. 12. Simulation results of i_d current, i_q current and motor speed comparison. (a) and (b) Method 1. (c) and (d) Method 2.

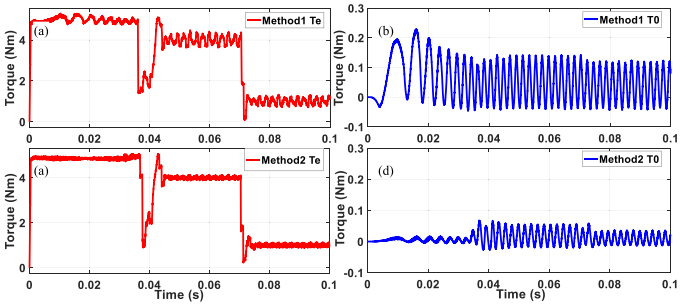

Fig. 13. Simulation results of the torque T_e and T_0 comparison. (a) and (b) Method 1. (c) and (d) Method 2.

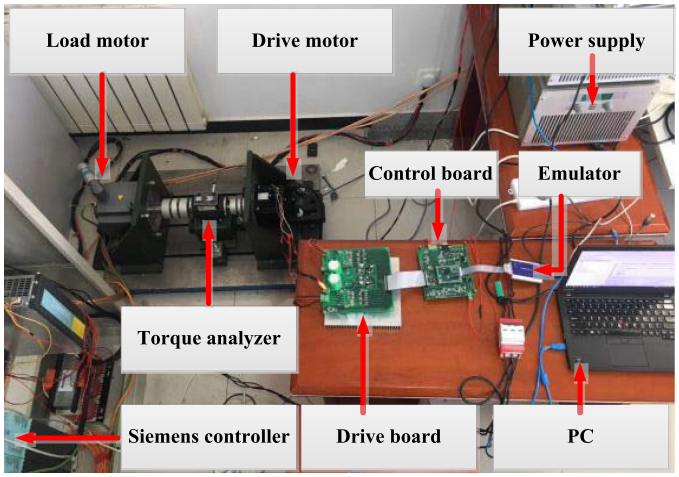

Fig. 14. Experimental platform of a two-level inverter 1 kW drive OEW-PMSM system.

i_{q0} is added in method 2 and counteract the fluctuant torque ripple T_0. Therefore, the proposed DPCC method can suppress the torque ripple effectively in simulation.

V. Experimental Results

In this section, the OEW-PMSM drive system is established. The experimental platform includes a power supply (310 V), 1 kW drive OEW-PMSM system, oscilloscope, XDSV200 emulator, load motor system, torque analyzer, and PC. The TMS320F28377d and FNC42060F-type IPM are chosen as the main control chip and power module, respectively. The OEW-PMSM drive system is presented in Fig. 14. Similar to the simulation, the dead time is set to 2.5 μs and control period

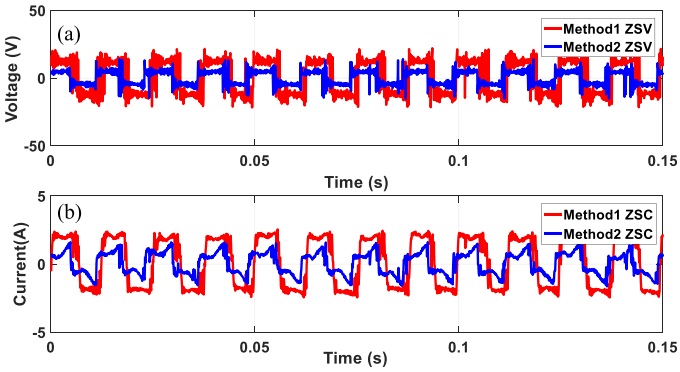

Fig. 15. Experimental results of ZSC i_0 and ZSV U_0 with 5 kHz cutoff frequency comparison at 400 r/min. (a) ZSV U_0. (b) ZSC i_0.

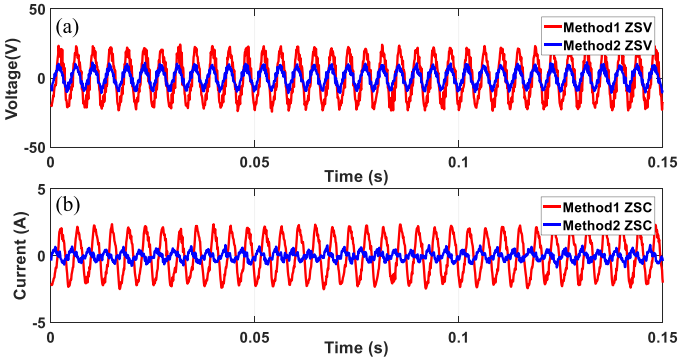

Fig. 16. Experimental results of ZSC i_0 and ZSV U_0 with 5 kHz cutoff frequency comparison at 1200 r/min. (a) ZSV U_0. (b) ZSC i_0.

is set to 50 μs. The traditional DPCC method (method 1) and the proposed DPCC method (method 2) are compared with different conditions. The speed closed-loop also adopts PI control and the PI proportionality coefficient and integral coefficient are 0.09 and 0.01, respectively. The SMC parameters k_{s0}, k_{s1}, and k_{g0} are 50, 50, and –2000, respectively.

Fig. 15 shows the ZSC and ZSV with 5 kHz cutoff frequency at 400 r/min in the two methods. From this figure, we can find that the value of ZSC in method 2 is lower than that of method 1. When the motor speed is at 1200 r/min, method 2 has the same suppression performance in Fig. 16. To testify the suppression performance for ZSC at different load torque conditions, Fig. 17 shows the ZSC and ZSV with 5 kHz cutoff frequency performance results and the load torque is set from 2 to 4 N·m and down to 3 N·m during the experiment. It can be seen that although the variation of load torque has a slight impact on the value of ZSC and ZSV, method 2 can suppress ZSC effectively at different speed and load torque conditions. In the proposed DPCC method, Fig. 18 shows the ZSO performance and it can be seen that the estimate ZSC and ZSV can track the actual ZSC and ZSV at different speed conditions. It should be noted that although the estimated ZSV is approximately equal to the actual average ZSV, there are variations between the estimated ZSV and actual ZSV within each control period. Fig. 19 shows i_d current, i_q current, and motor speed performance of the two methods at 800 r/min condition. The load torque is set from 2 to 4 N·m and then to 3 N·m and it can be

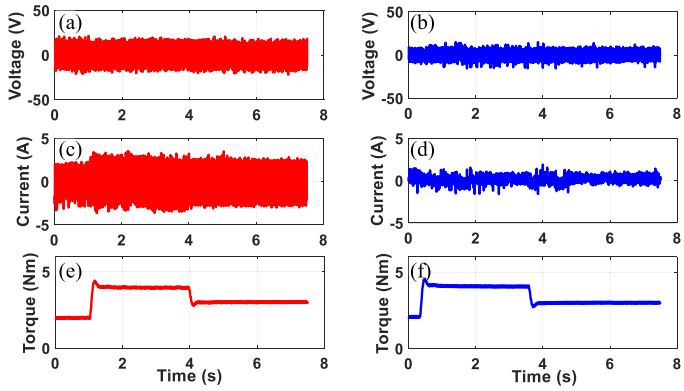

Fig. 17. Experimental results of the two methods comparison at 800 r/min. (a) ZSV U_0 with 5 kHz cutoff frequency in method 1. (b) ZSV U_0 with 5 kHz cutoff frequency in method 2. (c) ZSC i_0 in method 1. (d) ZSC i_0 in method 2. (e) Load torque T_l in method 1. (f) Load torque T_l in method 2.

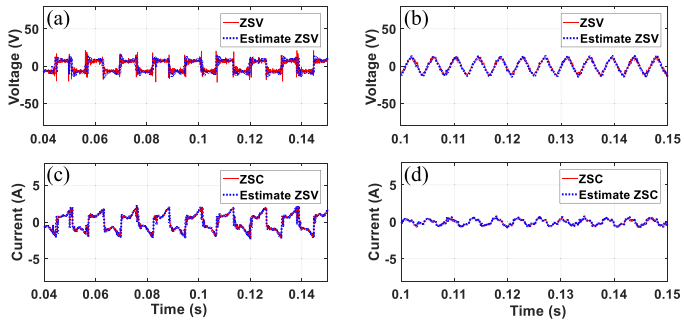

Fig. 18. Experimental results of the estimates of ZSC i_0 and ZSV U_0 comparison in method 2 at 400 and 1200 r/min, respectively. (a) ZSV with 5 kHz cutoff frequency and estimate of ZSV at 400 r/min. (b) ZSV with 5 kHz cutoff frequency and estimate of ZSV at 1200 r/min. (c) ZSC and estimate of ZSC at 400 r/min. (d) ZSC and estimate of ZSC at 1200 r/min.

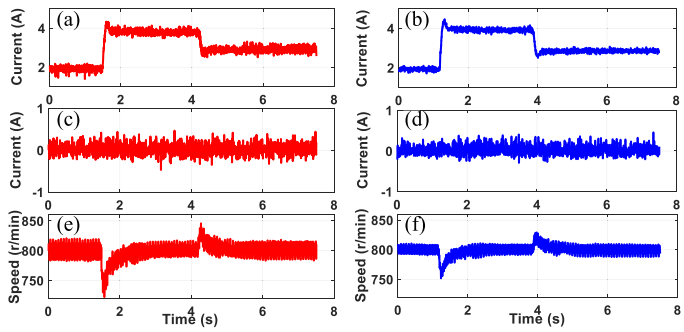

Fig. 19. Experimental results of i_q current, i_d current, and motor speed comparison. (a) i_q current in method 1. (b) i_q current in method 2. (c) i_d current in method 1. (d) i_d current in method 2. (e) Speed in method 1. (f) Speed in method 2.

seen that method 2 can suppress the fluctuation of the *dq*-axis currents and motor speed, which is similar to the results of simulation. In Fig. 20, the electromagnetic torque T_e performance of the two methods can be compared at 400 and 1200 r/min, respectively, and the load torque is set from 2 to 4 N·m during the experiment. It can be seen that the proposed DPCC method can suppress the torque ripple at different speed conditions. Zero-sequence back EMFs e_0 with no load are shown in Fig. 21, it can be seen that the zero-sequence back EMFs increase with

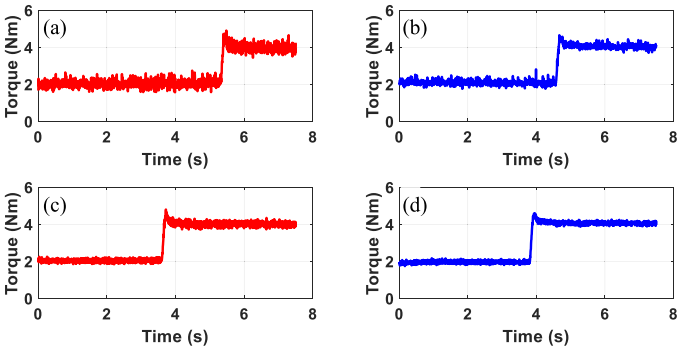

Fig. 20. Experimental results of the torque T_e comparison. (a) Method 1 at 400 r/min. (b) Method 2 at 400 r/min. (c) Method 1 at 1200 r/min. (d) Method 2 at 1200 r/min.

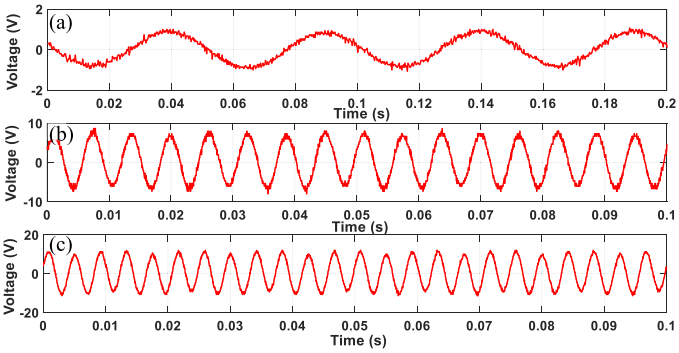

Fig. 21. Experimental results of the zero-sequence back EMF e_0 at different speed conditions. (a) e_0 at 100 r/min. (b) e_0 at 800 r/min. (c) e_0 at 1200 r/min.

the speed rising and the third-order harmonics in back EMF is almost equal to zero-sequence back EMFs at different speed conditions from the frequency spectrum analysis.

VI. Conclusion

The traditional DPCC method with SHCPWM will augment the ZSC and torque ripple. To deal with this problem, the academic contributions are summarized as follows.

1) This paper proposes a zero-sequence observer based on adaptive SMC to predict ZSV and ZSC simultaneously at the $k+1$th instant. From the simulation and experimental results of the proposed method, the estimates of ZSV and ZSC can track the actual ZSV and ZSC under different conditions.
2) A novel DPCC scheme with SHCPWM is proposed. From the results of the proposed method, the value of the ZSV and ZSC is reduced under different conditions compared with that of the traditional DPCC scheme with SHCPWM. In addition, since the injection of current i_{q0} can counteract the torque ripple to caused by zero-sequence EMF, we can see that the torque ripple is reduced under different conditions in the simulation and experimental results.

Therefore, the proposed DPCC scheme with SHCPWM has the capability of ZSC and torque ripple suppression and can be experimentally applied to OEW-PMSM drives.

References

[1] A. Kiadehi, K. Drissi, and C. Pasquier, "Adapted NSPWM for single DC-link dual-inverter fed open-end motor with negligible low-order harmonics and efficiency enhancement," *IEEE Trans. Power Electron.*, vol. 31, no. 12, pp. 8271–8281, Jan. 2016.

[2] C. Min and S. Dan, "A unified space vector pulse width modulation for dual two-level inverter system," *IEEE Trans. Power Electron.*, vol. 32, no. 2, pp. 889–893, Jun. 2016.

[3] V. T Somasekhar, S. Srinivas, and K. Gopakkumar, "A space vector based PWM switching scheme for the reduction of common-mode voltages for a dual inverter fed open-end winding induction motor drive," in *Proc. Power Electron. Spec. Conf.*, 2005, pp. 816–821.

[4] N. Bodo, M. Jones, and E. Levi, "A space vector PWM with common-mode voltage elimination for open-end winding five-phase drives with a single DC supply," *IEEE Trans. Ind. Electron.*, vol. 61, no. 5, pp. 2197–2207, Jul. 2013.

[5] S. Chowdhury, P. W Wheeler, C. Patel, and C. Gerada, "A multilevel converter with a floating bridge for open-end winding motor drive applications," *IEEE Trans. Ind. Electron.*, vol. 63, no. 9, pp. 5366–5375, Sep. 2016.

[6] R. U. Haque, A. Kowal, J. Ewanchuk, A. Knight, and J. Salmon, "PWM control of a dual inverter drive using an open-ended winding induction motor" in *Proc. IEEE Appl. Power Electron. Conf. Expo.*, Mar. 2013, pp. 150–156.

[7] Y. Zhou and H. Nian, "Zero-sequence current suppression strategy of open-winding PMSG system with common DC bus based on zero vector redistribution" *IEEE Trans. Ind. Electron.*, vol. 62, no. 6, pp. 3399–3408, Jun. 2015.

[8] A. M. Hava and E. Ün, "Performance analysis of reduced common-mode voltage PWM methods and comparison with standard PWM methods for three-phase voltage-source inverters," *IEEE Trans. Power Electron.*, vol. 24, no. 1, pp. 241–252, Jan. 2009.

[9] A. D. Kiadehi, K. E. K. Drissi, and C. Pasquier, "Angular modulation of dual-inverter fed open-end motor for electrical vehicle applications," *IEEE Trans. Power Electron.*, vol. 31, no. 4, pp. 2980–2990, Apr. 2016.

[10] V. T. Somasekhar, S. Srinivas, and B. R. Prakash, "Pulse width-modulated switching strategy for the dynamic balancing of zero-sequence current for a dual-inverter fed open-end winding induction motor drive," *Inst. Eng. Technol. Elect. Power Appl.*, vol. 1, no. 4, pp. 591–600, Jul. 2007.

[11] V. T. Somasekhar and S. Srinivas, "Effect of zero-vector placement in a dual-inverter fed open-end winding induction motor drive with alternate sub-hexagonal center PWM switching scheme," *IEEE Trans. Power Electron.*, vol. 23, no. 3, pp. 1584–1591, May 2008.

[12] V. T. Somasekhar and S. Srinivas, "Effect of zero-vector placement in a dual-inverter fed open-end winding induction-motor drive with a decoupled space-vector PWM strategy," *IEEE Trans. Ind. Electron.*, vol. 55, no. 6, pp. 2497–2505, Jun. 2008.

[13] Z. Wang, J. Chen, M. Cheng, and K. T. Chau, "Field-oriented control and direct torque control for paralleled VSIs fed PMSM drives with variable switching frequencies," *IEEE Trans. Power Electron.*, vol. 31, no. 3, pp. 2417–2428, Mar. 2016.

[14] B. J. Kang and C. M. Liaw, "A robust hysteresis current-controlled PWM inverter for linear PMSM driven magnetic suspended positioning system," *IEEE Trans. Ind. Electron.*, vol. 48, no. 5, pp. 956–967, Oct. 2001.

[15] R. Errouissi, M. Ouhrouche, H. Wen, and A. Trzynadlowski, "Robust cascaded nonlinear predictive control of a permanent magnet synchronous motor with antiwindup compensator," *IEEE Trans. Ind. Electron.*, vol. 59, no. 8, pp. 3078–3088, Aug. 2012.

[16] S. Vazquez, J. I. Leon, L. G. Franquelo, and J. Rodriguez, "Model predictive control: A review of its applications in power electronics," *IEEE Ind. Electron. Mag.*, vol. 8, no. 1, pp. 16–31, Mar. 2014.

[17] X. Zhang and K. Wang, "Current prediction based zero sequence current suppression strategy for the semi-controlled open-winding PMSM generation system with a common DC bus" *IEEE Trans. Ind. Elect.*, vol. 65, no. 8, pp. 6066–6076, Aug. 2018.

[18] E. K. M. Ravi, V. P. K. Kunisetti, and V. K. Thippiripati, "Enhanced predictive torque control for open end winding induction motor drive without weighting factor assignment," *IEEE Trans. Power Electron.*, vol. 34, no. 1, pp. 503–513, Jan. 2019, doi:10.1109/TPEL.2018.2812760.

[19] S. Chong, D. Sun, Z. Zheng, and H. Nian, "Simplified model predictive control for dual-inverter fed open-winding permanent magnet synchronous motor," *IEEE Trans. Energy Convers.*, vol. 33, no. 4, pp. 1846–1854, Dec. 2018, doi:10.1109/TEC.2018.2841012.

[20] B. Zhu, K. Rajashekara, and H. Kubo, "A novel predictive current control for open-end winding induction motor drive with reduced computation burden and enhanced zero sequence current suppression," in *Proc. Appl. Power Electron. Conf. Expo.*, May 2017, pp. 552–557.
[21] H. Zhan, Z. Q. Zhu, and M. Odavic, "Analysis and suppression of zero sequence circulating current in open winding PMSM drives with common DC bus," in *Proc. IEEE Energy Convers. Congr. Expo.*, Sep. 2016, pp. 1–8.
[22] H. Nian and W. Hu, "Torque ripple suppression method with reduced switching frequency for open-winding PMSM drives with common DC bus," *IEEE Trans. Ind. Electron.*, vol. 66, no. 1, pp. 674–684, Jan. 2019, doi: 10.1109/TIE.2018.2833803.
[23] H. Zhan, Z. Q. Zhu, and M. Odavic, "Nonparametric sensorless drive method for open-winding PMSM based on zero-sequence back EMF with circulating current suppression," *IEEE Trans. Power Electron.*, vol. 32, no. 5, pp. 3808–3817, May 2017.
[24] Q. An, J. Liu, and Z. Peng, "Dual-space vector control of open-end winding permanent magnet synchronous motor drive fed by dual inverter," *IEEE Trans. Power Electron.*, vol. 31, no. 12, pp. 8329–8342, Dec. 2016.
[25] R. Baranwal, K. Basu, and N. Mohan, "Carrier-based implementation of SVPWM for dual two-level VSI and dual matrix converter with zero common-mode voltage," *IEEE Trans. Power Electron.*, vol. 30, no. 3, pp. 1471–1487, Mar. 2015.
[26] P. Cortes, J. Rodriguez, C. Silva, and A. Flores, "Delay compensation in model predictive current control of a three-phase inverter," *IEEE Trans. Ind. Electron.*, vol. 59, no. 2, pp. 1323–1325, Feb. 2012.

Xin Yuan was born in Heilongjiang, China, in 1990. He received the B.Eng. and M.Sc. degrees in electrical engineering, in 2013 and 2016, respectively. He is currently working toward the Ph.D. degree in the National Engineering Laboratory for Electric Vehicles and the School of Mechanical Engineering, Beijing Institute of Technology, Beijing, China.

He is a Visiting Student in PEMC Group, University of Nottingham, Nottingham, U.K., since January 2019. His research interests include synchronous motor drives, multi-phase motor drives, and fault-tolerant strategy of motor.

Chengning Zhang received the M.E. degree in control theory and control engineering and the Ph.D. degree in vehicle engineering from the Beijing Institute of Technology, Beijing, China, in 1989 and 2001, respectively.

He is currently a Professor and the Vice Director with the National Engineering Laboratory for Electric Vehicles, Beijing Institute of Technology. His research interests include electric vehicles, vehicular electric motor drive systems, battery management systems, and chargers.

Shuo Zhang received the B.Eng. degree from the North China Institute of Aerospace Engineering, Hebei, China, in 2011, and the Ph.D. degree in vehicle engineering from the Beijing Institute of Technology, Beijing, China, in 2017.

He is currently an Assistant Professor with National Engineering Laboratory for Electric Vehicles and the School of Mechanical Engineering, Beijing Institute of Technology. His research interests include the modeling and control for the permanent magnet synchronous motors, multi-motor driving systems, and hybrid power systems.